Monsoonal Influence on Typhoon Morakot (2009). Part I: Observational Analysis

LIGUANG WU AND JIA LIANG

Key Laboratory of Meteorological Disaster of the Ministry of Education, Nanjing University of Information Science and Technology, Nanjing, China

CHUN-CHIEH WU

Department of Atmospheric Sciences, National Taiwan University, Taipei, Taiwan

(Manuscript received 12 November 2010, in final form 30 March 2011)

ABSTRACT

Typhoon Morakot made landfall on Taiwan with a record rainfall of 3031.5 mm during 6–13 August 2009. While previous studies have emphasized the influence of southwesterly winds associated with intraseasonal oscillations and monsoon surges on moisture supply, the interaction between Morakot and low-frequency monsoon flows and the resulting influence on the slow movement and asymmetric precipitation structure of the typhoon were examined observationally.

Embedded in multi-time-scale monsoonal flows, Morakot generally moved westward prior to its landfall on Taiwan and underwent a coalescence process first with a cyclonic gyre on the quasi-biweekly oscillation time scale and then with a cyclonic gyre on the Madden–Julian oscillation time scale. The coalescence enhanced the synoptic-scale southwesterly winds of Morakot and thus decreased its westward movement and turned the track northward, leading to an unusually long residence time in the vicinity of Taiwan. The resulting slow movement and collocation with the low-frequency gyres also maintained the major rainfall in southern Taiwan because the low-frequency flows played an important role in enhancing the winds on the southern side, especially during 6–9 August 2009. In addition to the lifting effect of the Taiwan terrain and the moisture supply associated with monsoon flows, the study suggests that the monsoonal influence maintained the major rainfall area in southern Taiwan through reducing the translation speed, shifting Morakot northward, and enhancing the low-frequency flows on the southern side of the typhoon. Since the enhanced low-frequency flows did not shift northward with the movement of Morakot, its primary rainfall expanded outward with time as the typhoon center moved northwestward after its landfall on Taiwan.

1. Introduction

About 90 tropical cyclones (TCs) develop over the world's oceans each year (Webster et al. 2005), and some make landfall in populous regions, causing heavy tolls in life and property (Pielke and Landsea 1998; Pielke et al. 2008; Zhang et al. 2009). The study of landfalling TCs has been conducted for decades through observational analysis and numerical simulation. Brand and Blelloch (1973) first observationally documented the effect of the Philippine Islands on the TC track, intensity, and size, followed by a series of idealized numerical simulations (e.g., Tuleya and Kurihara 1978; Chang 1982; Tuleya et al. 1984; Bender et al. 1985; Lin et al. 2002). With the advent of relatively sophisticated mesoscale numerical models, TCs that made landfall on Taiwan Island were investigated extensively (e.g., Yeh and Elsberry 1993a,b; Wu and Kuo 1999; Wu 2001; Wu et al. 2002; Chiao and Lin 2003; Chen and Yau 2003; Lin et al. 2005; Chien et al. 2008; Lee et al. 2008; Jian and Wu 2008; Yang et al. 2008; Wu et al. 2009). These numerical studies support that the topographic effect of the island can deflect TC tracks, modify the TC structure, and enhance TC rainfall. However, compared to the topographic

Corresponding author address: Dr. Liguang Wu, Pacific Typhoon Research Center, Key Laboratory of Meteorological Disaster of Ministry of Education, Nanjing University of Information Science and Technology, Nanjing, Jiangsu 210044, China.
E-mail: liguang@nuist.edu.cn

DOI: 10.1175/2011JAS3730.1

effect, relatively few studies have been conducted on the interaction between Asian monsoon systems and TCs although the interaction can lead to torrential rainfall over Taiwan (Chien et al. 2008; Wu et al. 2009).

The monsoon activity in the South China Sea and western North Pacific includes prominent atmospheric variability ranging from synoptic-scale tropical disturbances (Liebmann and Hendon 1990; Lau and Lau 1990; Chang et al. 1996) to the quasi-biweekly oscillation (QBW) (Murakami and Frydrych 1974; Murakami 1975; Kikuchi and Wang 2009) to the Madden–Julian oscillation (MJO) (Madden and Julian 1971, 1972; Wang and Rui 1990; Hsu and Weng 2001). The QBW and MJO are usually called tropical intraseasonal oscillations (ISOs). Studies have revealed that TC tracks alternate between clusters of straight and recurving paths with an intraseasonal time scale (Harr and Elsberry 1991; Harr and Elsberry 1995; Chen et al. 2009). Ko and Hsu (2006, 2009) found that the ISO westerly phase was closely associated with recurving TC tracks in the vicinity of Taiwan. A pioneering study conducted by Carr and Elsberry (1995) provides a clue as to how ISOs can alter the TC track and rainfall pattern. Using a barotropic vorticity equation model, Carr and Elsberry (1995) argued that many sudden track changes that typically consist of rapid slowing of westward movement and a substantial northward acceleration over the western North Pacific might be explained with the interaction between a TC and a monsoon gyre. The latter is a specific pattern of the evolution of the low-level monsoon circulation and can be identified as a nearly circular cyclonic vortex with a diameter of roughly 2500 km (Lander 1994). In their barotropic model, the coalescence of a TC with a monsoon gyre results in an area of high winds similar to the observed monsoon surge due to Rossby wave energy dispersion associated with the monsoon gyre.

Typhoon Morakot (2009) formed in the tropical western North Pacific on 3 August 2009 and made landfall over Taiwan late on 7 August 2009, leading to the worst flooding over the past 50 yr in southern Taiwan. Ge et al. (2010) and Hong et al. (2010) suggested that the record-breaking rainfall associated with Morakot resulted from the interaction between the typhoon and monsoon circulation. In addition to the topographic lifting effect associated with the Central Mountain Range (CMR), both Hong et al. (2010) and Ge et al. (2010) emphasized the abundant moisture supply from the southwesterly winds in the unprecedented rainfall event. While Hong et al. (2010) focused on the overlapping effect of the submonthly disturbance and 40–50-day ISO, Ge et al. (2010) mainly stressed the strong monsoon surge due to Rossby wave energy dispersion (Carr and Elsberry 1995).

In fact, the extreme rainfall associated with Morakot was accompanied with the highly asymmetric structure of convective activity and the reduced movement in the vicinity of Taiwan. Morakot took more than 2 days to pass through Taiwan and the Taiwan Strait while its major rainfall occurred in southern Taiwan. Two issues still remain to be addressed. First, why did Morakot stay in the vicinity of Taiwan for more than 2 days? And why did the major rainfall not shift with the northwestward movement of the typhoon? The objective of this study is to explore the monsoonal influence on the activity of Morakot, in particular on its highly asymmetric structure and slow movement in the vicinity of Taiwan. As the first part of this study, observational evidence will be presented about how the interaction between Morakot and low-frequency monsoon flows affect the movement and the associated asymmetric precipitation pattern of Morakot. The associated numerical study will be presented in the second part (Liang et al. 2011).

2. Data and analysis method

In this study the TC data are obtained from the Japan Meteorological Agency (JMA) and the Joint Typhoon Warning Center (JTWC) best-track datasets, which contain measurements of TC center positions (latitude and longitude) and intensity (maximum sustained wind speed and central pressure) at 6-h intervals. This study also employs the National Centers for Environmental Prediction (NCEP) Final (FNL) Operational Global Analysis data on $1.0° \times 1.0°$ grids at every 6 h. The Global Forecast System (GFS) is operationally run 4 times a day in the near-real time at NCEP. The data are available on the surface and at 26 pressure levels from 1000 to 10 hPa, including surface pressure, sea level pressure, geopotential height, temperature, relative humidity, and winds. The environmental flows associated with Morakot are basically derived from the FNL dataset.

The rainfall data associated with Typhoon Morakot are derived from two datasets. The first is the hourly precipitation observations from the automatic weather stations in Taiwan. The other is the 3-h TRMM rainfall data product (3B42) with a spatial resolution of $0.25° \times 0.25°$. The 3B42 product is a combined precipitation product based on the satellite microwave and infrared observations. The convective activity associated with Morakot is examined using the Atmospheric Infrared Sounder (AIRS) brightness temperature from the National Aeronautics and Space Administration (NASA) *Aqua* satellite (http://www.nasa.gov/mission_pages/hurricanes/archives/2009/past_years09.html), the radar reflectivity from Taiwan Central Weather Bureau, and the remapped color-enhanced infrared images of the

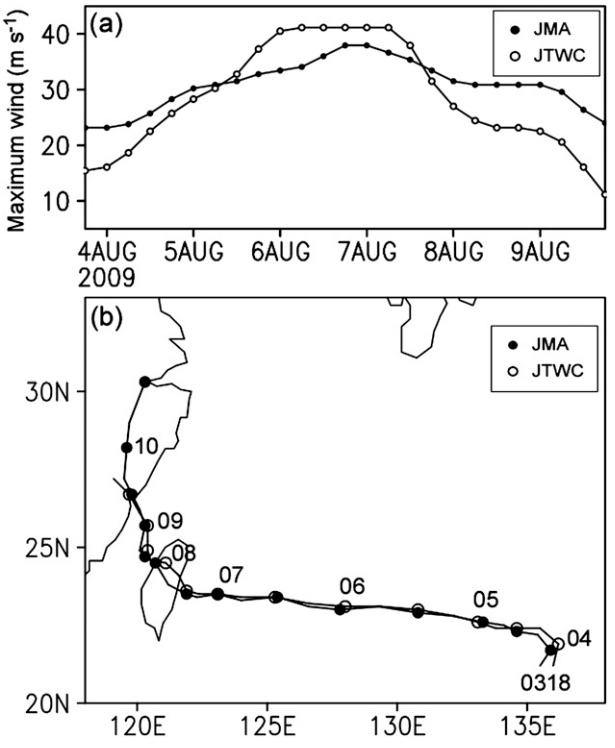

FIG. 1. (a) Time series of the intensity of Typhoon Morakot from the JMA and JTWC best-track datasets with 6-h intervals and (b) the corresponding tracks with dots and numbers indicating 12-h intervals and dates.

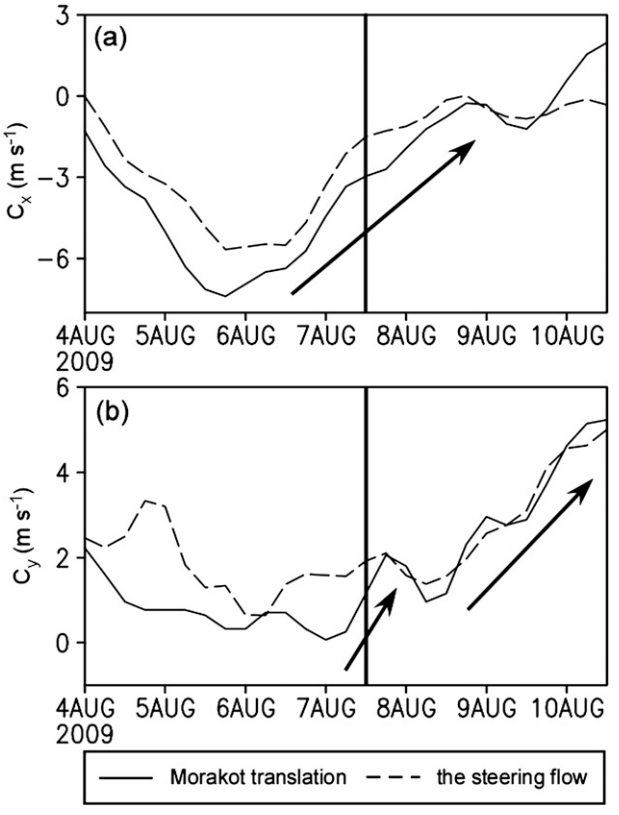

FIG. 2. Time series of (a) the zonal component C_x (m s^{-1}) and (b) the meridional component C_y (m s^{-1}) of the translation speed of Typhoon Morakot (solid) and the steering flow (dashed) with vertical lines indicating the landfall time and arrows schematically showing the trends in the translation speed and steering flow.

National Oceanic and Atmospheric Administration (NOAA) five geostationary satellites (http://rammb.cira.colostate.edu/).

To examine the influence of flows associated with Morakot on various time scales, we use Lanczos filters in time at each grid point. A low-pass filter with a 20-day cutoff period is used to isolate the MJO-scale flow and the background state. A bandpass filter with a 10–20-day period is used for the QBW-scale flow. The synoptic-scale flow is the difference between the unfiltered flow and the flow from a 10-day low-pass filter. For convenience, we call these components the MJO, QBW, and synoptic time scale components in this study. It should be pointed out that the inner typhoon structure cannot be represented in the FNL data because of its relatively low horizontal resolution.

3. Distinctive features of Typhoon Morakot (2009)

a. Track change

Figure 1 shows the intensity of Morakot and its track based on the JTWC and JMA best-track data from 1800 UTC 3 August to 1200 UTC 10 August 2009. A tropical depression formed during early 2 August 2009 in the Philippine Sea. It strengthened into a tropical storm and was named Morakot at 1800 UTC 3 August by JMA (Fig. 1a). Morakot then intensified into a severe tropical storm at 1200 UTC 4 August and a typhoon at 1800 UTC 5 August. The JTWC data shows that the system attained its peak intensity of 40 m s^{-1} before it made landfall on Taiwan around 1200 UTC 7 August. It degraded into a tropical storm before making the second landfall over mainland China on 9 August.

As shown in Fig. 1b, Morakot started to turn northwestward as it made landfall on Taiwan late on 7 August. It stayed off the eastern coast of Taiwan for about 12 h, took 9 h to cross the island, and moved into the Taiwan Strait on August 8. In the Taiwan Strait, the typhoon turned and took a generally northward track. Because of its slow movement, Morakot took 31 h to cross the strait before landing in Fujian Province at 0600 UTC 9 August. Morakot lingered for 52 h in the vicinity of Taiwan. Such a long residence time is not common for those storms that make landfall on the island.

The zonal translation speed of Morakot underwent a significant change during 6–7 August (Fig. 2a). The

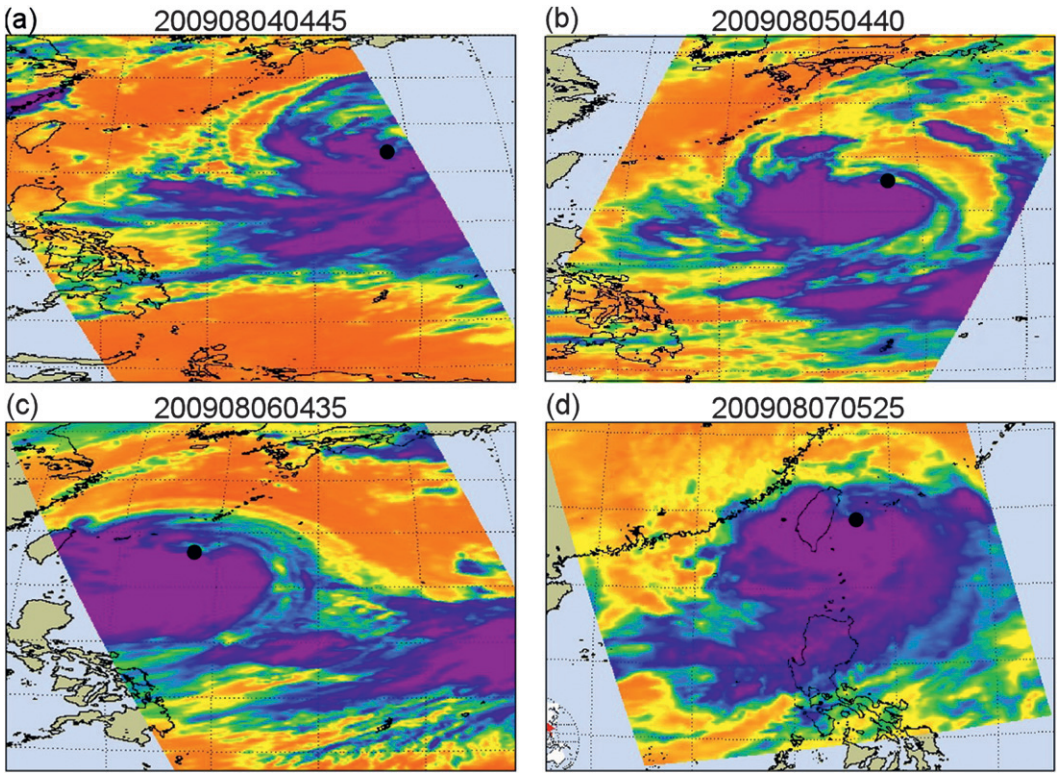

FIG. 3. AIRS brightness temperature from the NASA *Aqua* satellite at (a) 0445 UTC 4 Aug, (b) 0440 UTC 5 Aug, (c) 0435 UTC 6 Aug, and (d) 0525 UTC 7 Aug 2009, respectively. The areas colder than −53° and −37°C are respectively purple and blue, with black dots indicating the approximate position of Morakot's center (downloaded from http://www.nasa.gov/mission_pages/hurricanes/archives/2009/past_years09.html).

typhoon accelerated westward by 1800 UTC 6 August and then decelerated. It moved very slowly when it entered the Taiwan Strait around 0000 UTC 9 August. In general Morakot moved westward with a small meridional speed by 0000 UTC 7 August (Fig. 2b), when it was located to the east of Taiwan. The typhoon started to accelerate northward on 7 August. We can divide the track of Morakot into three segments: 1) generally westward movement from 4 to 7 August, 2) crossing Taiwan Island and the Taiwan Strait from 7 to 9 August, and 3) making a second landfall over mainland China from 9 to 10 August. The corresponding mean translation speeds are 5.4, 2.6, and 4.4 m s^{-1}, respectively, for the three periods. Compared to the first period, the translation speed was reduced by a factor of 2 during the second period. That was why Morakot stayed more than 2 days in the vicinity of Taiwan Island.

It has been known that a TC is largely steered by the large-scale environmental flow and the ventilation flow that results from the interaction between the TC and its environment (Holland 1983; Carr and Williams 1989; Fiorino and Elsberry 1989; Wu and Wang 2000, 2001a,b). In this study the steering flow is calculated as the mass-weighted mean wind averaged within a radius of 440 km (4° latitudes) between 850 and 300 hPa. As shown in Fig. 2, the calculated steering is reasonably consistent with the typhoon translation speeds. It is suggested that the slow-down of Morakot's movement and the northward deflections of its track during 7–9 August were mainly a result of the change in the steering flow.

b. Highly asymmetric structure of convection

Here we use the convective area to roughly show the horizontal structure of the convection of Morakot. The cloud-top temperature, which is usually associated with deep convection, can measure activity of convection associated with a TC. Figure 3 shows the AIRS cloud-top temperature associated with Morakot. The blue and purple colors in this figure indicate the area with temperature lower than 240 and 220 K, respectively. On 4 August, the deep convection mainly occurred south of the center of Morakot (Fig. 3a). AIRS captured the whole inner region of Morakot on 5 August. The cold cloud top less than 240 K (blue) covered an area about half of the AIRS swath width, about 850 km in diameter (Fig. 3b). However, the blue area stretched over the

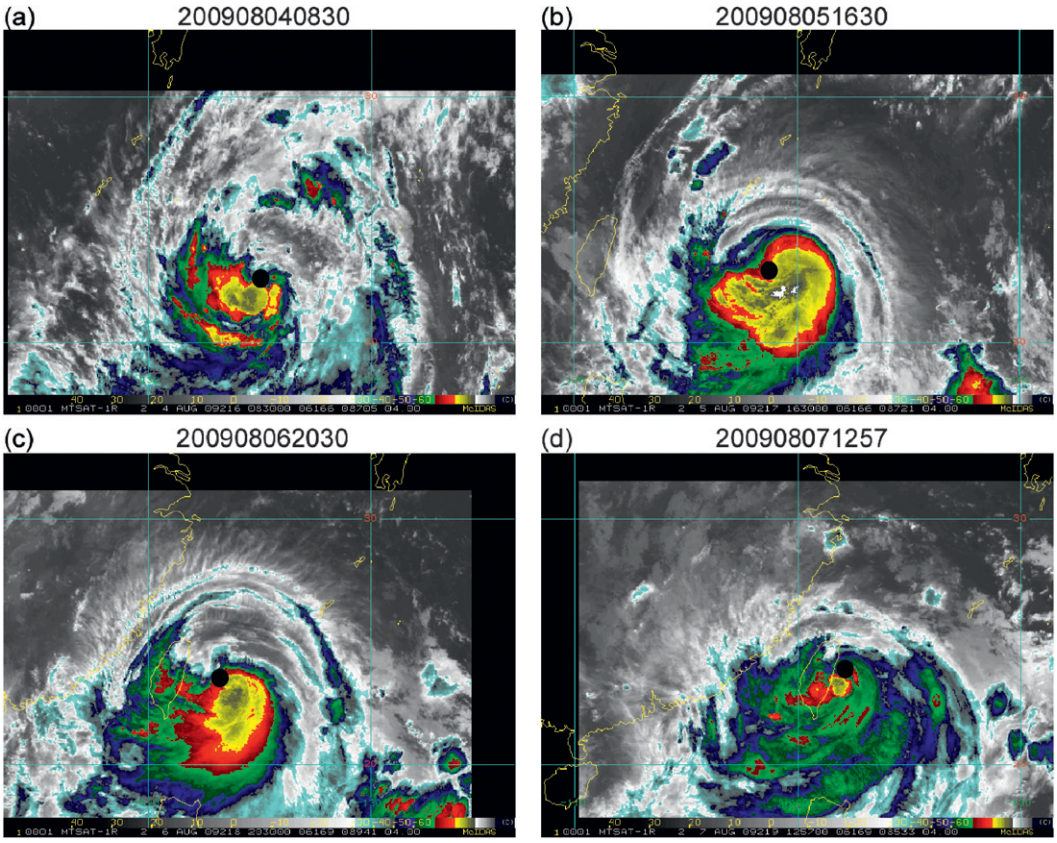

FIG. 4. Remapped color enhanced infrared imagery from the geostationary Multifunctional Transport Satellites (MTSAT-IR) with a 4-km resolution at (a) 0830 UTC 4 Aug, (b) 1630 UTC 5 Aug, (c) 2030 UTC 6 Aug, and (d) 1257 UTC 7 Aug 2009. The blue area denotes brightness temperatures less than 223 K, with black dots indicating the center of Typhoon Morakot (downloaded from http://rammb.cira.colostate.edu/).

whole AIRS swath, about 1600 km in diameter on 6 and 7 August (Figs. 3c,d). Compared with 5 August, the deep convective area indicated with the purple increased significantly on 6 August, mainly on the southern side of the typhoon circulation.

The convective asymmetry associated with Morakot can also be demonstrated with the NOAA enhanced infrared imagery that was remapped from the infrared satellite imagery (~11 μm) of five geostationary satellites (Fig. 4). The blue area corresponds to the cold cloud top with a temperature less than 223 K. On 4 August (Fig. 4a), the cold cloud associated with Morakot was about 500 km in size. The area was enlarged significantly by 1630 UTC 5 August. The convective activity was primarily enhanced on the southern side of the typhoon. A separate cloud band was clearly observed to the southeast of the typhoon center on 7 August when its center was just off the eastern coast of Taiwan. The radar reflectivity shows more details of the convective structure of Morakot (Fig. 5). In addition to the high asymmetric rainbands on the southern side, this figure indicates that no closed eyewall was observed during its landfall over the Taiwan Island. The significant precipitation occurred in the outer rainbands, 200–400 km south of the typhoon center.

c. *Extreme rainfall*

Figure 6 shows the accumulated rainfall from 0000 UTC 4 August to 0000 UTC 13 August 2009. Morakot produced very heavy rainfall in southern Taiwan, leading to the worst flooding over the past 50 yr. Its total accumulated precipitation was as much as 3031.5 mm at the Weiliaoshan station on the Sandimen Mountains, Pingtung County. The extreme rainfall set a new record for typhoon precipitation in Taiwan, surpassing the previous one of 1736 mm, created by Typhoon Herb (1996). Despite the category-1 intensity of Morakot, the extreme amount of rainfall within such a short period triggered enormous mudslides and severe flooding in Taiwan (Hong et al. 2010).

As shown in Fig. 6, it is clear that southern Taiwan experienced the heaviest rainfall of Morakot. The area with accumulated rainfall above 2800 mm can be found

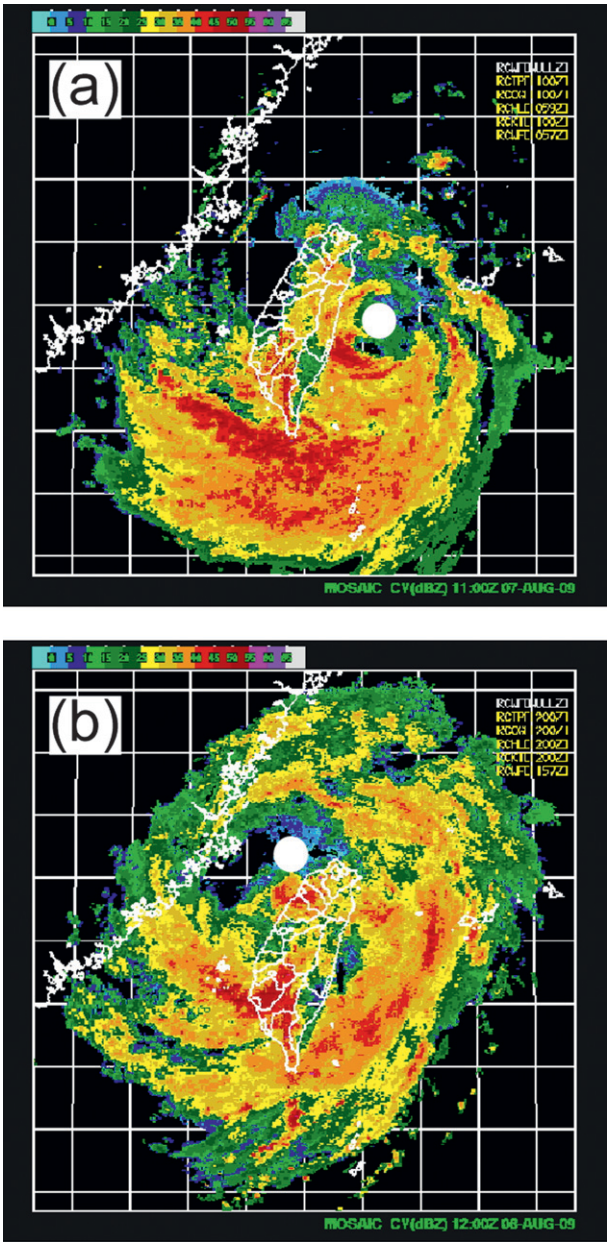

FIG. 5. Radar reflectivity associated with Morakot from Taiwan Central Weather Bureau at (a) 1100 UTC 7 Aug and (b) 1200 UTC 8 Aug 2009, with white dots indicating the center of Typhoon Morakot.

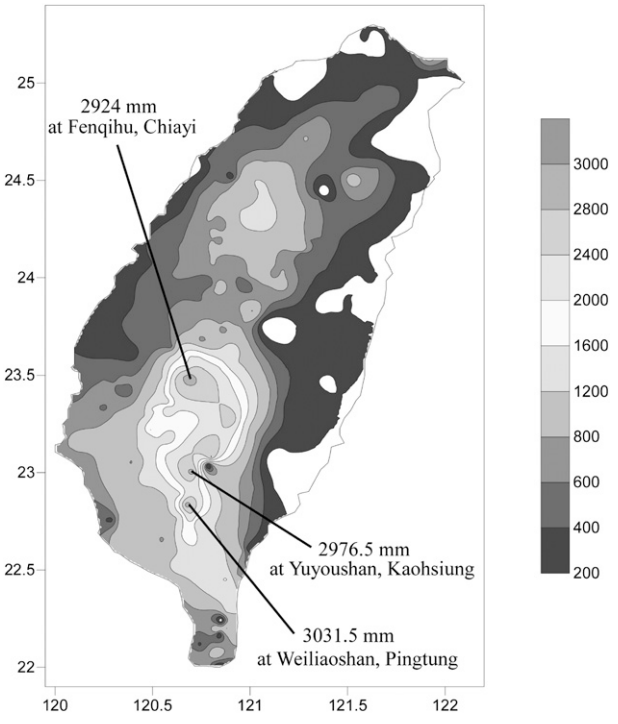

FIG. 6. The observed accumulated rainfall (mm) from 0000 UTC 4 Aug to 0000 UTC 13 Aug 2009. The marked positions indicate the three maximum rainfall centers.

in southern Taiwan. We further examine the daily accumulated rainfall during the period 4–12 August (figure not shown). On 4–5 August, Morakot was more than 1000 km away from Taiwan, and the rainfall mainly in northern Taiwan resulted from the outer rainband. On 6 August, 24 h before the typhoon made landfall over Taiwan, heavy rainfall started to be observed in southern Taiwan, while the rainfall in northern Taiwan was enhanced with a maximum of 286.5 mm. On 7–9 August when Morakot made landfall over Taiwan and moved into the Taiwan Strait, the rainfall mainly occurred over southern Taiwan. The maximum accumulated precipitation was 1003.5, 1402.0, and 963.0 mm, respectively. The 1402.0-mm rainfall was observed at Weiliaoshan of Pingtung County on 8 August. After the typhoon made the second landfall over mainland China on 9 August, significant rainfall was still observed in southern Taiwan with a maximum of 423 mm. The rainfall in Taiwan decreased significantly after 11 August 2009.

Figure 7 shows the hourly rainfall at Weiliaoshan of Pingtung County from 0000 UTC 6 August to 0000 UTC 13 August. It is clear that the precipitation had two phases at the station. The first phase ranged from 1800 UTC 06 August to 1400 UTC 9 August, during which Morakot approached, made landfall over, and crossed Taiwan Island, and entered the Taiwan Strait. The maximum hourly precipitation of 115 mm occurred at 1000 UTC 8 August, when the typhoon center was located about 300 km to the northwest of Weiliaoshan, just off the western coast of the island. The second phase corresponded with a relatively weak precipitation process from 1500 UTC 9 August to 0000 UTC 13 August. The maximum hourly precipitation reached 60 mm at 1400 UTC 10 August, more than 1 day after Morakot made the

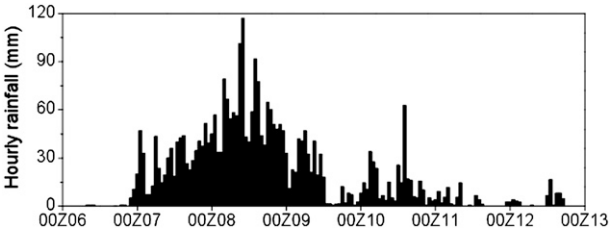

FIG. 7. Time series of the hourly rainfall (mm) associated with Typhoon Morakot at Weiliaoshan, Pingtung County, from 0000 UTC 6 Aug to 0000 UTC 13 Aug 2009.

second landfall over mainland China. Figure 7 indicates that the extremely heavy rainfall of 3031.5 mm at Weiliaoshan was associated with two separate phases while the most rainfall occurred from 1800 UTC 6 August to 1400 UTC 9 August. Figure 8 further shows the 48-h observed rainfall (mm) from 0000 UTC 7 August 2009 to 0000 UTC 9 August 2009. During this period, the maximum rainfall was observed at Fenqihu, Chiayi, while the rainfall was 2540.0 mm at Weiliaoshan, accounting for 83.8% of the total precipitation associated with Morakot.

While Ge et al. (2010) and Hong et al. (2010) focused mainly on the enhanced southwesterly flow to the south of the typhoon center and the associated moisture supply, we argue that its unusually long residence time in the vicinity of Taiwan and highly asymmetric convective structure are responsible for the extreme rainfall event associated with Morakot in southern Taiwan.

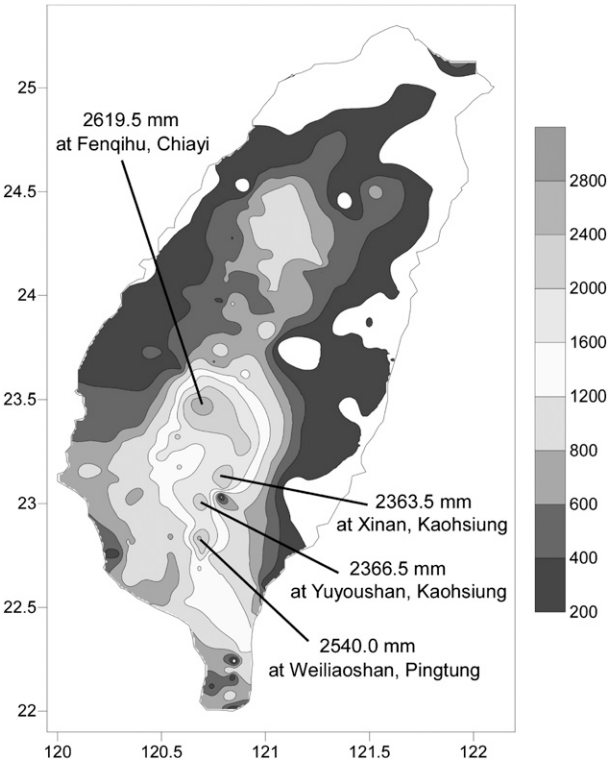

FIG. 8. The observed accumulated rainfall (mm) associated with Typhoon Morakot from 0000 UTC 7 Aug to 0000 UTC 9 Aug 2009. The marked positions indicate the three centers of the accumulated rainfall.

4. The evolution of ISO flows associated with Typhoon Morakot

In this section, the filtered winds are used to illustrate the evolution of low-frequency flows associated with Morakot. Figure 9 shows the 700-hPa ISO wind fields prior to and during landfalling on Taiwan Island. Note that the seasonal mean (July–September) winds have been removed from the MJO flows to make the low-frequency gyre outstanding. This figure clearly shows the coalescence of the typhoon with the QBW and MJO gyres, respectively.

On the QBW time scale (Figs. 9a–c), a cyclonic gyre can be seen just off the eastern coast of the Taiwan Island at 0600 UTC 6 August and 0600 UTC 7 August, and its center moved to the western coast of the island at 0600 UTC 8 August. Morakot was generally located to the east of the gyre center and underwent a coalescence process with the gyre. When the typhoon made landfall over Taiwan, it was almost concentric with the QBW gyre. At 0600 UTC 8 August, Morakot moved to the western coast of Taiwan Island and remained concentric with the gyre. On the MJO time scale (Figs. 9d–f), a monsoon gyre can be seen off the western coast of Taiwan Island. Embedded in the monsoon gyre, Morakot also underwent a coalescence process with the MJO-scale cyclonic gyre. The typhoon was nearly concentric with the monsoon gyre when moved into the Taiwan Strait at 0600 UTC 8 August (Fig. 9f). In response to the two coalescence processes with the QBW and MJO gyres, Morakot turned northwestward when it made landfall on Taiwan and farther northward when it moved into the Taiwan Strait, respectively (Fig. 1b).

5. The influence of ISO flows on Typhoon Morakot

Based on the above analysis, we can find that the extreme rainfall associated with Morakot concurred with the coalescence processes, in which Morakot tended to approach the centers of the MJO and QBW gyres. In the meantime, the enlarging area of deep convection occurred mainly to the south of the typhoon center. Moreover, the maximum hourly rainfall was observed on 8 August when Morakot was nearly collocated with the MJO and QBW gyres. It is suggested that the low-frequency gyres play an important role in the record-breaking rainfall event.

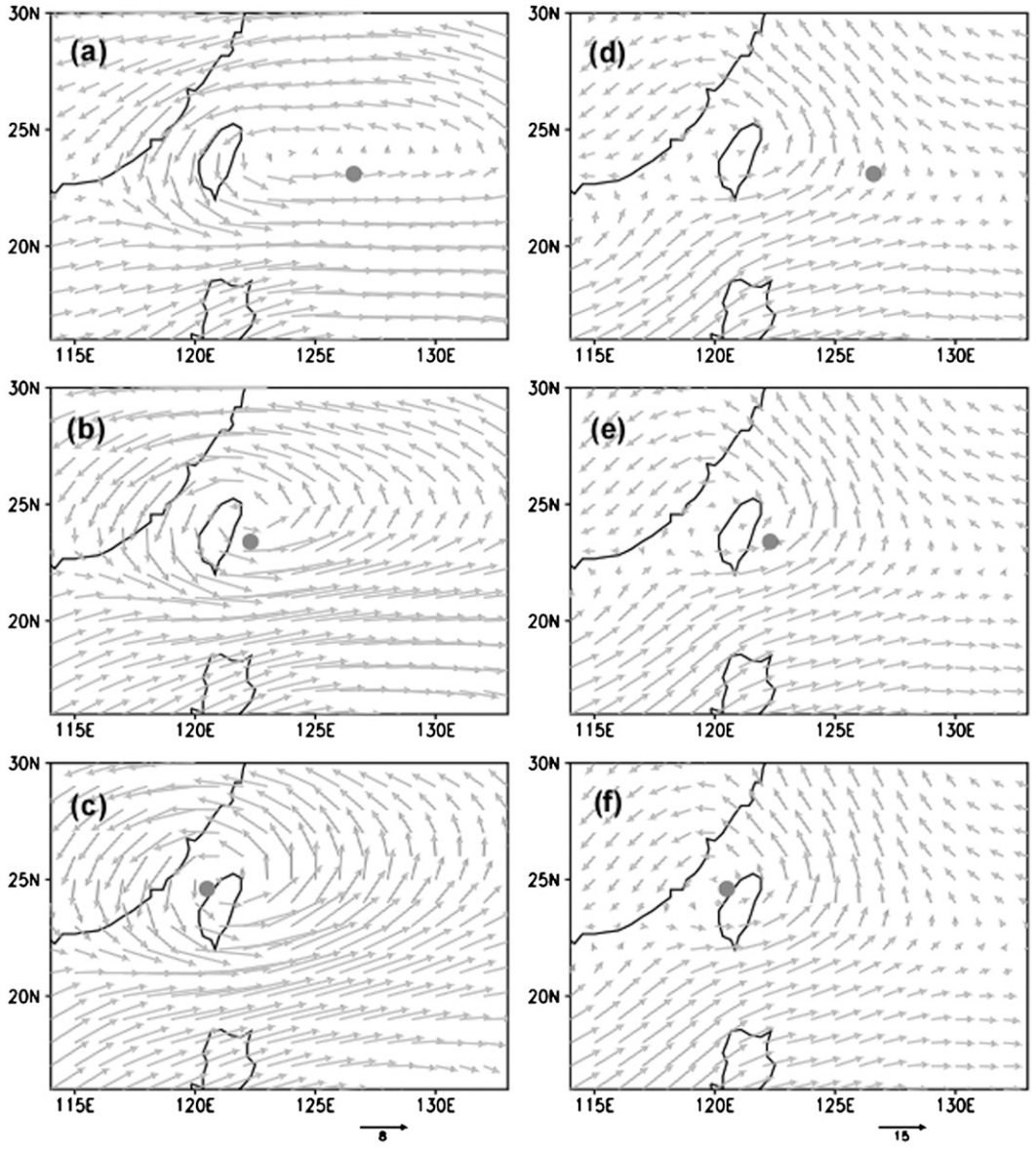

FIG. 9. The 700-hPa winds (m s^{-1}) on the (a)–(c) QBW and (d)–(f) MJO time scales at (a),(d) 0600 UTC 6 Aug, (b),(e) 0600 UTC 7 Aug, and (c),(f) 0600 UTC 8 Aug 2009, with gray dots indicating the center of Morakot.

As Morakot approached the centers of the low-frequency gyres, the pressure gradient increased, enhancing southwesterly winds to its southeast. Figure 10 shows the unfiltered 700-hPa FNL winds associated with the typhoon. At 1200 UTC 6 August (Fig. 10a), the enhanced winds (more than 25 m s^{-1}) appeared primarily to the northeast of the typhoon center with relatively strong southwesterly flow extending southward over the Philippine Sea. At 1200 UTC 7 August just before the typhoon made landfall over Taiwan, Morakot reached its peak intensity in the JTWC dataset and its wind structure became relatively symmetric (Fig. 10b). The maximum winds of more than 30 m s^{-1} were observed to the south of the typhoon center. At 1200 UTC 8 August when the typhoon became nearly concentric with the low-frequency gyres, the wind structure became rather asymmetric with enhanced southwesterly winds extending northeastward from the South China Sea to the Pacific Ocean (Fig. 10c). The enhancement of southwesterly winds, accompanied by the coalescence process of Morakot with both of the MJO and QBW gyres, is consistent with previous studies (Carr and Elsberry 1995; Ge et al. 2010).

Using a barotropic vorticity equation model, Carr and Elsberry (1995) found that tropical cyclones coalesce with the monsoon gyre and then exhibit a sudden

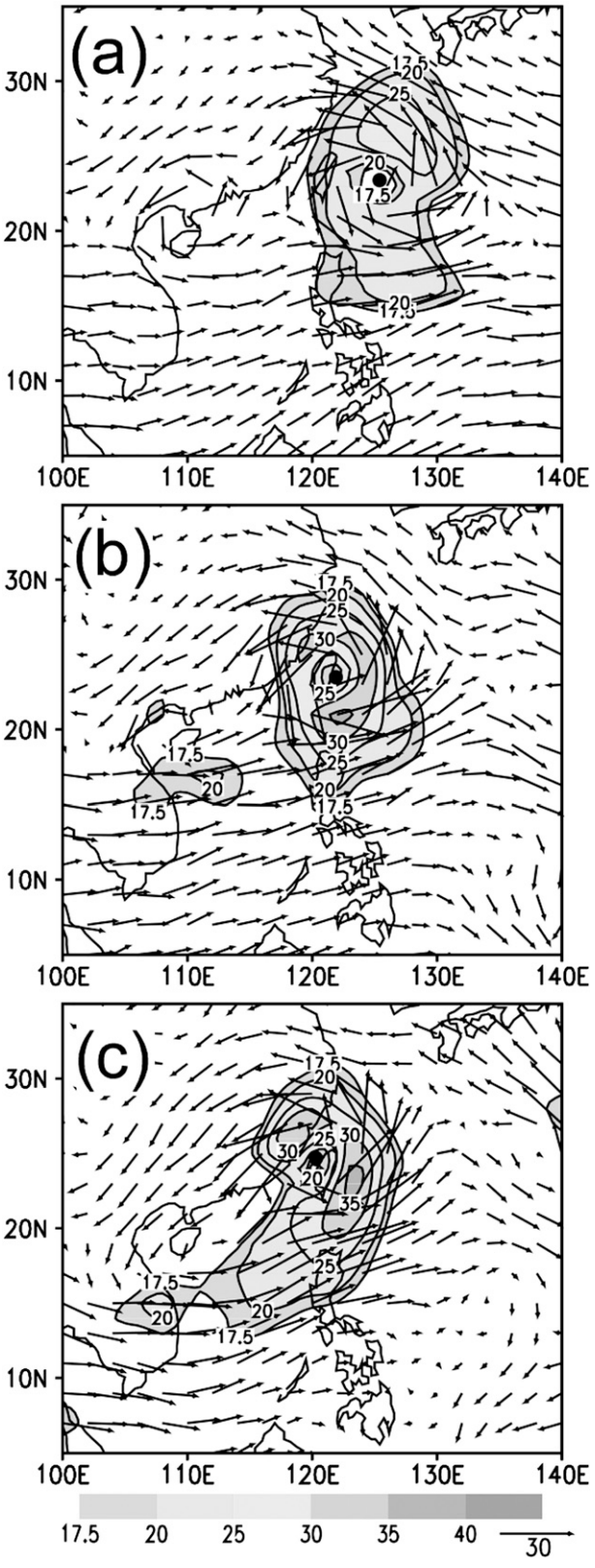

FIG. 10. The 700-hPa unfiltered FNL wind (m s^{-1}) at (a) 1200 UTC 6 Aug, (b) 1200 UTC 7 Aug, and (c) 1200 UTC 8 Aug 2009, with black dots indicating the position of the typhoon center. The shaded area indicates wind speeds exceeding 17.5 m s^{-1}.

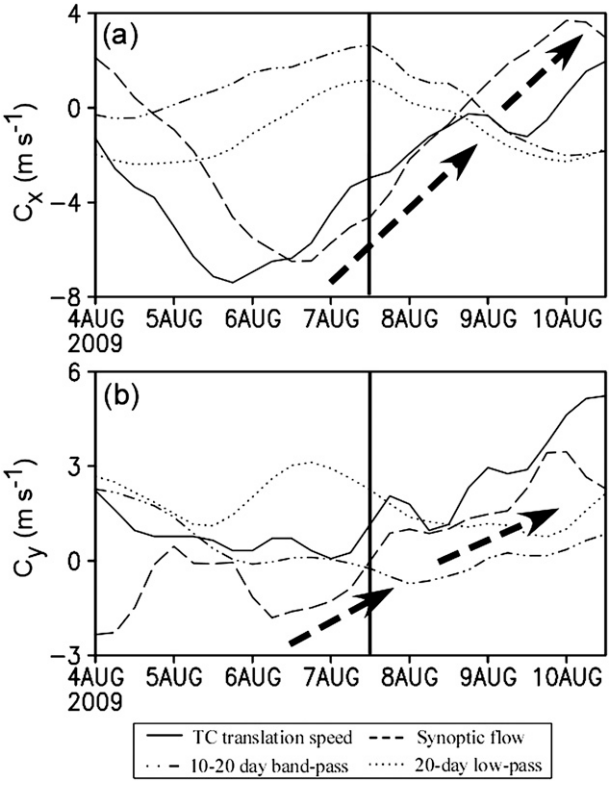

FIG. 11. Time series of (a) C_x (m s^{-1}) and (b) C_y (m s^{-1}) of the translation speed (solid) of Morakot and the associated steering components calculated from the 10-day high-pass, 10–20-day bandpass, and 20-day low-pass filtered winds. The vertical lines and arrows indicate the landfall time and the schematic trend of the synoptic-scale steering, respectively.

northward track change, which is very similar to the sudden poleward track changes observed in the western North Pacific. During the coalescence phase, the weak monsoon gyre undergoes a β-induced dispersion, producing ridging to the east and southeast of the tropical cyclone and an intermediate region of high southerly winds that resemble the observed monsoon surge. Wu et al. (2011) provided observational evidence to show that the low-frequency gyre can act as the idealized monsoon gyre in the experiments of Carr and Elsberry (1995). They found that the sudden track changes occurred near the center of the MJO-scale cyclonic circulation or at the bifurcation point of the steering flows at 700 hPa and were all associated with a well-developed QBW-scale cyclonic gyre. The feature of the QBW-scale flow was also observed in the case of Typhoon Morakot.

To verify this, we calculated the contribution of different time-scale steering flows to the typhoon movement (Fig. 11). As the winds were enhanced on the southern side of the typhoon, the westward movement started to slow down before landfall. The synoptic-scale

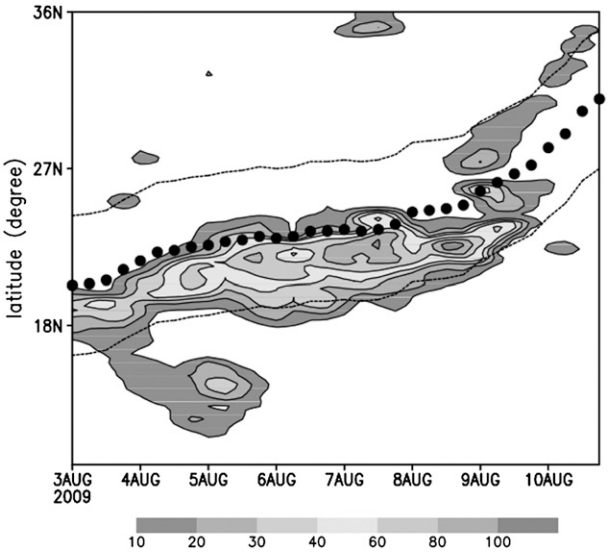

FIG. 12. The time–latitude cross section of the 6-h TRMM accumulated rainfall (3B42, mm) along the longitude of Morakot's center. The shaded areas indicate the 6-h accumulated rainfall exceeding 10 mm. The black dots and two dashed lines indicate the positions of the typhoon center and 440 km away from the typhoon center, respectively.

steering flow started to reduce the westward movement of Morakot late on 6 August and its contribution became eastward on 9 August. In the meridional direction, the contribution of the synoptic-scale steering flow first reduced the southward movement during 6–7 August and then enhanced the northward movement during 8–10 August. Thus, the enhanced synoptic-scale flow was responsible for the northward track shift and slow movement of Morakot in the vicinity of Taiwan and the low-frequency gyres affect the track change of Morakot through the enhanced synoptic winds.

However, the maximum rainfall did not shift much as the typhoon moved northward into the Taiwan Strait. Figure 12 shows the time–latitude cross section of the 6-h TRMM rainfall along the longitude of the typhoon center. The rainfall was mostly on the southern side within 440 km from the typhoon center. The relative distance of the maximum rainfall from the typhoon center decreased prior to 6 August but started to increase with time when Morakot moved to the east of Taiwan late on 6 August. On late 7 August when Morakot was about to make landfall, the maximum precipitation occurred about 100 km from the typhoon center, but about 300 km on 9 August. It is clear that the maximum rainfall associated with Morakot remained in southern Taiwan as the typhoon moved northward.

One may argue that the southward dominance of the rainfall was associated with the vertical wind shear, since many studies showed that in response to vertical wind shear the structure of the tropical cyclone eyewall region becomes significantly asymmetric with a dominant azimuthal wavenumber-1 component (e.g., Jones 1995; Wang and Holland 1996; Bender 1997; Reasor et al. 2000; Frank and Ritchie 1999, 2001; Wu and Wang 2001a,b; Black et al. 2002; Rogers et al. 2003; Zhu et al. 2004; Braun et al. 2006; Wu and Braun 2004). Frank and Ritchie (1999) found that when the grid was saturated and the explicit moisture scheme dominated in their simulation, the upward motion and precipitation shifted to the downshear-left quadrant. Figure 13 shows the relationship between the vertical wind shear averaged over a radius of 440 km and the 6-h TRMM rainfall. During the period 4–7 August, in agreement with previous studies, an enhanced precipitation area within 200 km was generally located to the downshear-left quadrant. However, the vertical wind shear decreased significantly since 1800 UTC 8 August after Morakot made landfall over Taiwan. The enhanced precipitation generally occurred about 300 km away from the typhoon center (Figs. 14g,h). Thus, the enhanced rainfall to the south of the typhoon center was not a direct result of the vertical wind shear.

So why did the primary rainfall area shown in Fig. 8 remain in southern Taiwan or why did the maximum rainfall shown in Fig. 12 shift outward while Morakot made landfall, crossed Taiwan Island, and entered the Taiwan Strait during 7–9 August? To answer this question, we plot the time–latitude cross section of the 700-hPa winds along the longitude of the typhoon center (Fig. 14). Note that this figure can only show the evolution of the outer winds of Morakot due to the horizontal resolution of the FNL data. As shown in Fig. 14a, the maximum winds on the southern side were reached late on 7 August, just prior to the landfall. The timing agrees with the best-track data shown in Fig. 1a. While the winds on the northern side were dominated by the synoptic-scale flows, the low-frequency flows played an important role in enhancing the winds on the southern side, in agreement with Hong et al. (2010). Two maxima of the synoptic-scale winds on the southern side can be found in Fig. 14b. The one that occurred just prior to the landfall may result from the intensification of Morakot, but it is also likely that the enhanced synoptic-scale winds were a result of the interaction between the typhoon and the QBW gyre. The wind maximum on late 9 August might result primarily from the enhanced pressure gradient because at this time Morakot became nearly concentric with the QBW and MJO gyres (Fig. 9), suggesting the influence of the low-frequency flows on the enhanced synoptic-scale flow on the southern side of the typhoon.

The QBW-scale flows on the southern side increased steadily since the formation of Morakot and reached the

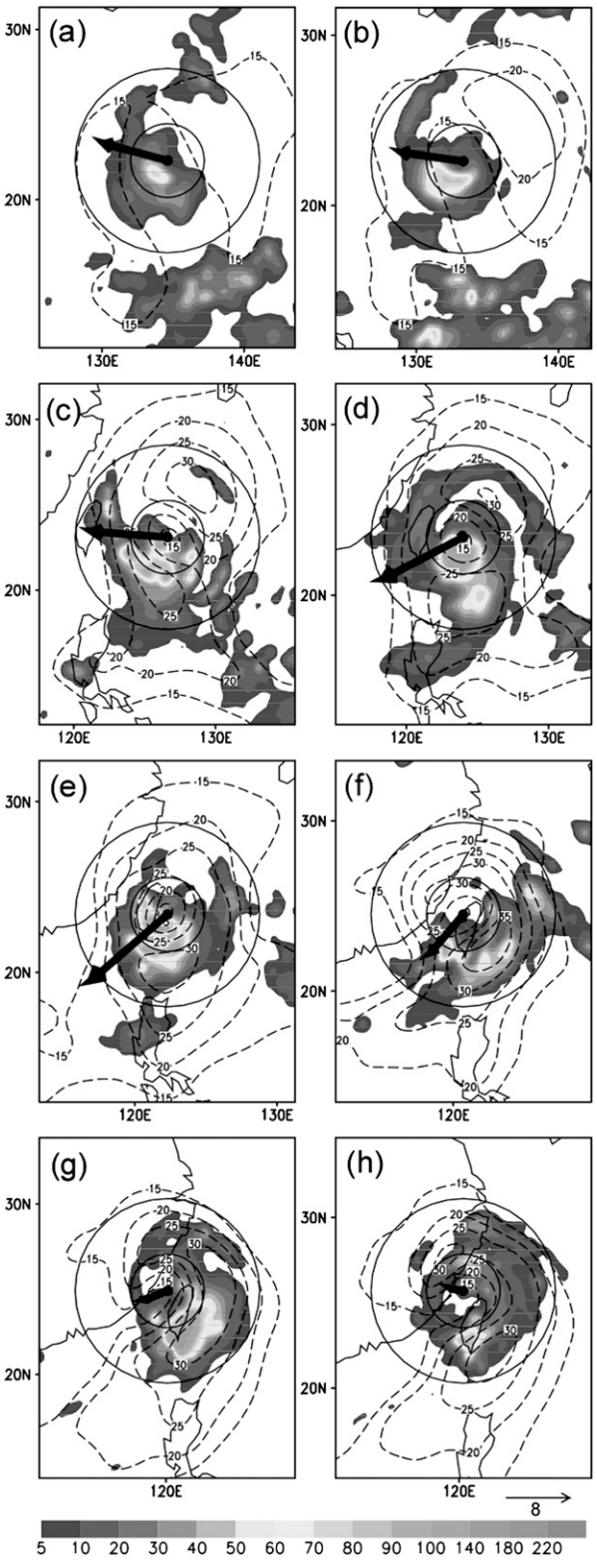

maximum around 8 August with the appearance of the QBW-scale anticyclone to the southeast (not shown). The MJO-scale flows increased quickly when the typhoon approached the Taiwan Island by 8 August and the center of the MJO-scale gyre in the Taiwan Strait. The enhanced area of the low-frequency flows did not shift northward (Figs. 14c,d), whereas the enhanced synoptic-scale winds were closely associated with the northward shift of the typhoon (Fig. 14b). The increase in the relative distance of the enhanced low-frequency flows to the typhoon center is consistent with the relative shift in the main rainfall area shown in Fig. 12, suggesting the important role of the low-frequency flows in the extreme rainfall event. Hong et al. (2010) identified the contribution of the southwesterly low-frequency flows to the moisture convergence along the southwestern coast of Taiwan and the transportation of the moisture upslope of the CMR.

6. Summary

With a peak intensity of about 40 m s^{-1}, Typhoon Morakot made landfall over Taiwan late on 7 August 2009 and stayed more than 2 days over the island and in the Taiwan Strait, leading to record-breaking rainfall in southern Taiwan. While previous studies have focused on the influence of southwesterly winds associated with ISOs and the monsoon surge caused by the Rossby wave energy dispersion of the typhoon on moisture supply (Hong et al. 2010; Ge et al. 2010), we examined observationally the interaction of Morakot with the low-frequency flows and the associated influence on the movement and precipitation structure of Morakot. In this study, analysis of various available datasets indicates that two roles of the interaction might have played in the extreme typhoon-related rainfall event.

First, the interaction between the low-frequency monsoon flows and Typhoon Morakot led to a northward shift in its track and a slowing down in its translation. Embedded in the low-frequency monsoon gyre,

←

FIG. 13. The 6-h TRMM accumulated rainfall (mm, shaded) with contours of less than 5 mm suppressed and the 700-hPa FNL wind speeds (m s^{-1}, dashed contours) with intervals of 5 m s^{-1} at (a) 1200 UTC 4 Aug, (b) 0000 UTC 5 Aug, (c) 0600 UTC 6 Aug, (d) 1800 UTC 6 Aug, (e) 0600 UTC 7 Aug, (f) 0000 UTC 8 Aug, (g) 1800 UTC 8 Aug, and (h) 0000 UTC 9 Aug 2009, respectively. The arrows indicate the vectors of the vertical wind shear between 200 and 850 hPa averaged over a radius of 440 km from the center of Morakot. The two circles are 200 and 500 km away from the typhoon center, respectively.

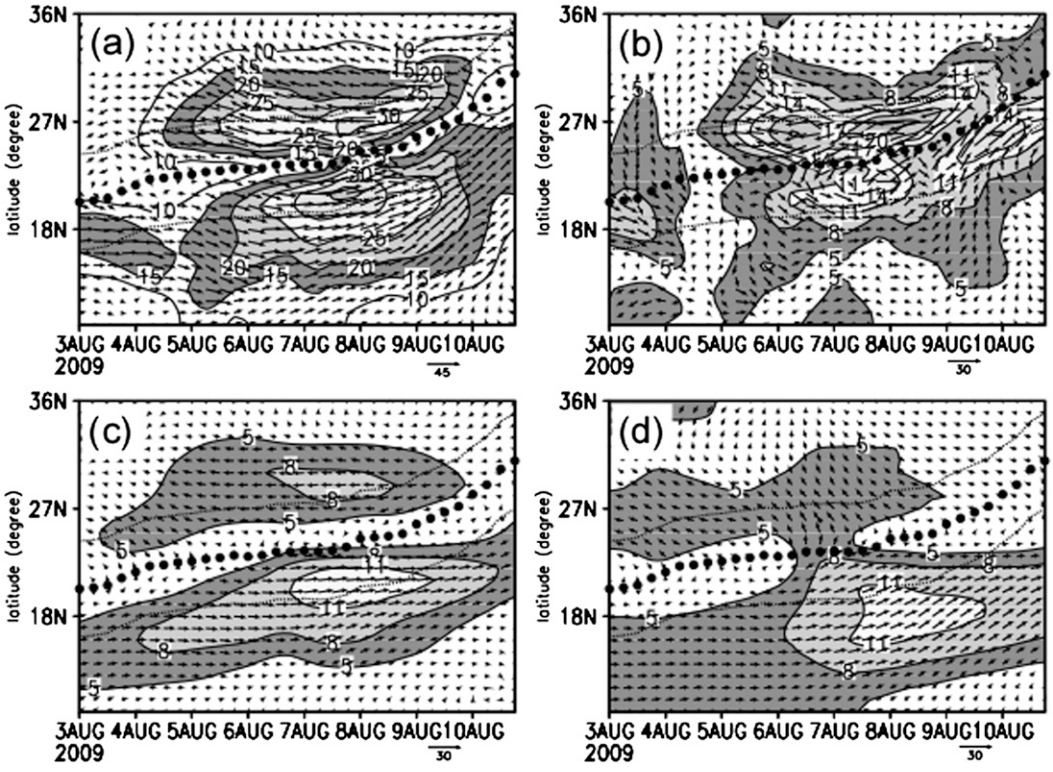

FIG. 14. Time–latitude cross sections of 700-hPa wind vectors and speeds (contour, m s^{-1}) for (a) the unfiltered, (b) 10-day high-pass, (c) 10–20-day bandpass, and (d) 20-day low-pass winds along the longitude of the center of Typhoon Morakot. The contours with speeds less than 10 m s^{-1} in (a) and 5 m s^{-1} in others are omitted. The intervals are 5 m s^{-1} in (a) and 3 m s^{-1} in others. The black dots and two dashed lines indicate the positions of the typhoon center and 440 km away from the typhoon center, respectively.

Morakot generally moved westward prior to its landfall on Taiwan and underwent a coalescence process first with a QBW-scale cyclonic gyre just off the eastern coast of Taiwan and then with the MJO-scale cyclonic gyre after entering the Taiwan Strait. The coalescence enhanced the synoptic-scale southwesterly winds on the southern side of Morakot and reduced its westward movement, leading to an unusually long residence time of the typhoon in the vicinity of Taiwan.

Second, the resulting slow movement and collocation with the ISO gyres maintained the major rainfall in the southern Taiwan. While the winds on the northern side were dominated by the synoptic-scale flows, the low-frequency flows played an important role in enhancing the winds on the southern side, especially during 6–9 August 2009, in agreement with Hong et al. (2010). The QBW-scale flows on the southern side increased steadily as the typhoon underwent a coalescence process with the QBW-scale cyclonic gyre, while the MJO-scale flows increased quickly when the typhoon approached the center of the MJO gyre in the Taiwan Strait. The enhanced low-frequency flows did not shift northward with Morakot.

In addition to the importance of the lifting effect of the terrain associated with the CMR and the abundant moisture supply associated with low-frequency monsoon flows and monsoon surges, this observational study suggests that the interaction of low-frequency monsoon flows with Morakot played an important role in the record-breaking rainfall event. The interaction maintained the major rainfall area in the southern Taiwan through reducing the translation speed, shifting Morakot northward and enhancing the low-frequency flows on the southern side of the typhoon.

Acknowledgments. This research was jointly supported by the National Basic Research Program of China (2009CB421503), the National Natural Science Foundation of China (Grant 40875038), the Social Commonweal Research Program of the Ministry of Science and Technology of China (GYHY200806009), and the Research Innovation Program for college graduates of Jiangsu Province (CX10B_290Z). The third author is supported by Grant NSC97-2111-M-002-016-MY3.

REFERENCES

Bender, M. A., 1997: The effect of relative flow on the asymmetric structures in the interior of hurricanes. *J. Atmos. Sci.,* **54,** 703–724.

——, R. E. Tuleya, and Y. Kurihara, 1985: A numerical study of the effect of a mountain range on a landfalling tropical cyclone. *Mon. Wea. Rev.,* **113,** 567–582.

Black, M. L., J. F. Gamache, F. D. Marks Jr., C. E. Samsury, and H. E. Willoughby, 2002: Eastern Pacific Hurricanes Jimena of 1991 and Olivia of 1994: The effect of vertical shear on structure and intensity. *Mon. Wea. Rev.,* **130,** 2291–2312.

Brand, S., and J. W. Blelloch, 1973: Changes in the characteristics of typhoons crossing the Philippines. *J. Appl. Meteor.,* **12,** 104–109.

Braun, S. A., M. T. Montgomery, and Z. Pu, 2006: High-resolution simulation of Hurricane Bonnie (1998). Part I: The organization of eyewall vertical motion. *J. Atmos. Sci.,* **63,** 19–42.

Carr, L. E., and R. T. Williams, 1989: Barotropic vortex stability to perturbations from axisymmetry. *J. Atmos. Sci.,* **46,** 3177–3191.

——, and R. L. Elsberry, 1995: Monsoonal interactions leading to sudden tropical cyclone track changes. *Mon. Wea. Rev.,* **123,** 265–290.

Chang, C.-P., J. Chen, P. Harr, and L. Carr, 1996: Northwestward-propagating wave patterns over the tropical western North Pacific during summer. *Mon. Wea. Rev.,* **124,** 2245–2266.

Chang, S. W.-J., 1982: The orographic effects induced by an island mountain range on propagating tropical cyclones. *Mon. Wea. Rev.,* **110,** 1255–1270.

Chen, T.-C., S.-Y. Wang, M.-C. Yen, and A. J. Clark, 2009: Impact of the intraseasonal variability of the western North Pacific large-scale circulation on tropical cyclone tracks. *Wea. Forecasting,* **24,** 646–666.

Chen, Y., and M. K. Yau, 2003: Asymmetric structures in a simulated landfalling hurricane. *J. Atmos. Sci.,* **60,** 2294–2312.

Chiao, S., and Y.-L. Lin, 2003: Numerical modeling of an orographically enhanced precipitation event associated with Tropical Storm Rachel over Taiwan. *Wea. Forecasting,* **18,** 325–344.

Chien, F.-C., Y.-C. Liu, and C.-S. Lee, 2008: Heavy rainfall and southwesterly flow after the leaving of Typhoon Mindulle (2004) from Taiwan. *J. Meteor. Soc. Japan,* **86,** 17–41.

Fiorino, M., and R. L. Elsberry, 1989: Some aspects of vortex structure related to tropical cyclone motion. *J. Atmos. Sci.,* **46,** 975–990.

Frank, W. M., and E. A. Ritchie, 1999: Effects on environmental flow upon tropical cyclone structure. *Mon. Wea. Rev.,* **127,** 2044–2061.

——, and ——, 2001: Effects of vertical wind shear on the intensity and structure of numerically simulated hurricanes. *Mon. Wea. Rev.,* **129,** 2249–2269.

Ge, X., T. Li, S. Zhang, and M. Peng, 2010: What causes the extremely heavy rainfall in Taiwan during Typhoon Morakot (2009)? *Atmos. Sci. Lett.,* **11,** 46–50, doi:10.1002/asl.255.

Harr, P. A., and R. L. Elsberry, 1991: Tropical cyclone track characteristics as a function of large-scale circulation anomalies. *Mon. Wea. Rev.,* **119,** 1448–1468.

——, and ——, 1995: Large-scale circulation variability over the tropical western North Pacific. Part I: Spatial patterns and tropical cyclone characteristics. *Mon. Wea. Rev.,* **123,** 1225–1246.

Holland, G. J., 1983: Tropical cyclone motion: Environmental interaction plus a beta effect. *J. Atmos. Sci.,* **40,** 328–342.

Hong, C.-C., M.-Y. Lee, H.-H. Hsu, and J.-L. Kuo, 2010: Role of submonthly disturbance and 40–50 day ISO on the extreme rainfall event associated with Typhoon Morakot (2009) in southern Taiwan. *Geophys. Res. Lett.,* **37,** L08805, doi:10.1029/2010GL042761.

Hsu, H.-H., and C.-H. Weng, 2001: Northwestward propagation of the intraseasonal oscillation in the western North Pacific during the boreal summer: Structure and mechanism. *J. Climate,* **14,** 3834–3850.

Jian, G.-J., and C.-C. Wu, 2008: A numerical study of the track deflection of Supertyphoon Haitang (2005) prior to its landfall in Taiwan. *Mon. Wea. Rev.,* **136,** 598–615.

Jones, S. C., 1995: The evolution of vortices in vertical shear. Part I: Initially barotropic vortices. *Quart. J. Roy. Meteor. Soc.,* **121,** 821–851.

Kikuchi, K., and B. Wang, 2009: Global perspective of the quasi-biweekly oscillation. *J. Climate,* **22,** 1340–1359.

Ko, K.-C., and H.-H. Hsu, 2006: Sub-monthly circulation features associated with tropical cyclone tracks over the East Asian monsoon area during July–August season. *J. Meteor. Soc. Japan,* **84,** 871–889.

——, and ——, 2009: ISO modulation on the submonthly wave pattern and the recurving tropical cyclones in the tropical western North Pacific. *J. Climate,* **22,** 582–599.

Lander, M. A., 1994: Description of a monsoon gyre and its effects on the tropical cyclones in the western North Pacific during August 1991. *Wea. Forecasting,* **9,** 640–654.

Lau, K.-H., and N.-C. Lau, 1990: Observed structure and propagation characteristics of tropical summertime synoptic-scale disturbances. *Mon. Wea. Rev.,* **118,** 1888–1913.

Lee, C.-S., Y.-C. Liu, and F.-C. Chien, 2008: The secondary low and heavy rainfall associated with Typhoon Mindulle (2004). *Mon. Wea. Rev.,* **136,** 1260–1283.

Liang, J., L. Wu, X. Ge, and C.-C. Wu, 2011: Monsoonal influence on Typhoon Morakot (2009). Part II: Numerical study. *J. Atmos. Sci.,* **68,** 2222–2235.

Liebmann, B., and H. H. Hendon, 1990: Synoptic-scale disturbances near the equator. *J. Atmos. Sci.,* **47,** 1463–1479.

Lin, Y.-L., D. B. Ensley, S. Chiao, and C.-Y. Huang, 2002: Orographic influence on rainfall and track deflection associated with the passage of a tropical cyclone. *Mon. Wea. Rev.,* **130,** 2929–2950.

——, S.-Y. Chen, C. M. Hill, and C.-Y. Huang, 2005: Control parameters for the influence of a mesoscale mountain range on cyclone track continuity and deflection. *J. Atmos. Sci.,* **62,** 1849–1866.

Madden, R. A., and P. R. Julian, 1971: Detection of a 40–50-day oscillation in the zonal wind in the tropical Pacific. *J. Atmos. Sci.,* **28,** 702–708.

——, and ——, 1972: Description of global-scale circulation cells in tropics with a 40–50-day period. *J. Atmos. Sci.,* **29,** 1109–1123.

Murakami, M., 1975: Cloudiness fluctuations during summer monsoon. *J. Meteor. Soc. Japan,* **54,** 175–181.

——, and M. Frydrych, 1974: On the preferred period of upper wind fluctuations during the summer monsoon. *J. Atmos. Sci.,* **31,** 1549–1555.

Pielke, R. A., Jr., and C. W. Landsea, 1998: Normalized hurricane damages in the United States: 1925–95. *Wea. Forecasting,* **13,** 621–631.

——, J. Gratz, C. W. Landsea, D. Collins, M. A. Saunders, and R. Musulin, 2008: Normalized hurricane damage in the United States: 1900–2005. *Nat. Hazards Rev.,* **9,** 29–42.

Reasor, P. D., M. T. Montgomery, F. D. Marks Jr., and J. F. Gamache, 2000: Low-wave number structure and evolution of the hurricane inner core observed by airborne dual-Doppler radar. *Mon. Wea. Rev.,* **128,** 1653–1680.

Rogers, R., S. Chen, J. Tenerelli, and H. Willoughby, 2003: A numerical study of the impact of vertical shear on the distribution of rainfall in Hurricane Bonnie (1998). *Mon. Wea. Rev.,* **131,** 1577–1599.

Tuleya, R. E., and Y. Kurihara, 1978: A numerical simulation of the landfall of tropical cyclones. *J. Atmos. Sci.,* **35,** 242–257.

——, M. A. Bender, and Y. Kurihara, 1984: A simulation study of the landfall of tropical cyclones using a movable nested-mesh model. *Mon. Wea. Rev.,* **112,** 124–136.

Wang, B., and H. Rui, 1990: Synoptic climatology of transient tropical intraseasonal convection anomalies: 1975–1985. *Meteor. Atmos. Phys.,* **44,** 43–61.

Wang, Y., and G. J. Holland, 1996: Tropical cyclone motion and evolution in vertical shear. *J. Atmos. Sci.,* **53,** 3313–3332.

Webster, P. J., G. J. Holland, J. A. Curry, and H.-R. Chang, 2005: Changes in tropical cyclone number, duration, and intensity in a warming environment. *Science,* **309,** 1844–1846.

Wu, C.-C., 2001: Numerical simulation of Typhoon Gladys (1994) and its interaction with Taiwan terrain using the GFDL hurricane model. *Mon. Wea. Rev.,* **129,** 1533–1549.

——, and Y.-H. Kuo, 1999: Typhoons affecting Taiwan: Current understanding and future challenges. *Bull. Amer. Meteor. Soc.,* **80,** 67–80.

——, T.-H. Yen, Y.-H. Kuo, and W. Wang, 2002: Rainfall simulation associated with Typhoon Herb (1996) near Taiwan. Part I: The topographic effect. *Wea. Forecasting,* **17,** 1001–1015.

——, K. K. W. Cheung, and Y.-Y. Lo, 2009: Numerical study of the rainfall event due to interaction of Typhoon Babs (1998) and the northeasterly monsoon. *Mon. Wea. Rev.,* **137,** 2049–2064.

Wu, L., and B. Wang, 2000: A potential vorticity tendency diagnostic approach for tropical cyclone motion. *Mon. Wea. Rev.,* **128,** 1899–1911.

——, and ——, 2001a: Movement and vertical coupling of adiabatic baroclinic tropical cyclones. *J. Atmos. Sci.,* **58,** 1801–1814.

——, and ——, 2001b: Effects of convective heating on movement and vertical coupling of tropical cyclones: A numerical study. *J. Atmos. Sci.,* **58,** 3639–3649.

——, and S. A. Braun, 2004: Effects of environmentally induced asymmetries on hurricane intensity: A numerical study. *J. Atmos. Sci.,* **61,** 3065–3081.

——, H. Zong, and J. Liang, 2011: Observational analysis of sudden tropical cyclone track changes in the vicinity of the East China Sea. *J. Atmos. Sci.,* in press.

Yang, M.-J., D.-L. Zhang, and H.-L. Huang, 2008: A modeling study of Typhoon Nari (2001) at landfall. Part I: Topographic effects. *J. Atmos. Sci.,* **65,** 3095–3115.

Yeh, T.-C., and R. L. Elsberry, 1993a: Interaction of typhoons with the Taiwan orography. Part I: Upstream track deflections. *Mon. Wea. Rev.,* **121,** 3193–3213.

——, and ——, 1993b: Interaction of typhoons with the Taiwan orography. Part II: Continuous and discontinuous tracks across the island. *Mon. Wea. Rev.,* **121,** 3213–3233.

Zhang, Q., L. Wu, and Q. Liu, 2009: Tropical cyclone damages in China 1983–2006. *Bull. Amer. Meteor. Soc.,* **90,** 489–495.

Zhu, T., D.-L. Zhang, and F. Weng, 2004: Numerical simulation of Hurricane Bonnie (1998). Part I: Eyewall evolution and intensity changes. *Mon. Wea. Rev.,* **132,** 225–241.